Electronic Supplementary Information for

A new family of two-dimensional ferroelastic semiconductors with negative Poisson's ratio

Jun-Hui Yuan,[1,+] Ge-Qi Mao,[1,+] Kan-Hao Xue,[1,*] Jiafu Wang[2,3] and Xiang-Shui Miao[1]

[1]Wuhan National Laboratory for Optoelectronics, School of Optical and Electronic Information, Huazhong University of Science and Technology, Wuhan 430074, China

[2]School of Science, Wuhan University of Technology, Wuhan 430070, China

[3]Department of Computer Science, Erik Jonsson School of Engineering and Computer

Science, University of Texas at Dallas, Richardson, TX 75080, USA

Corresponding Author, E-mail: **xkh@hust.edu.cn** (K.-H. Xue)

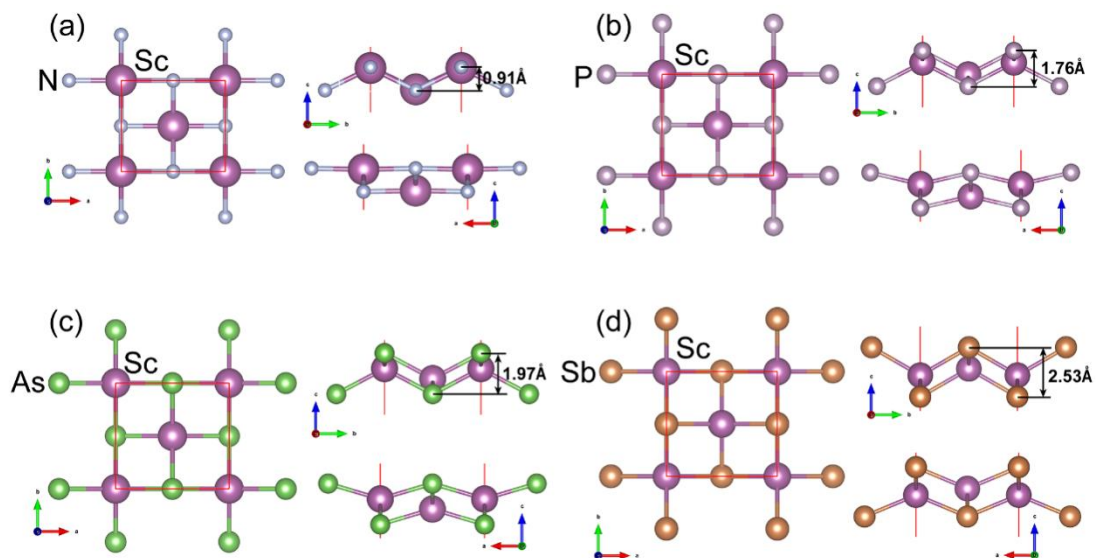[+]The authors J.-H. Yuan and G.-Q. Mao contributed equally to this work.

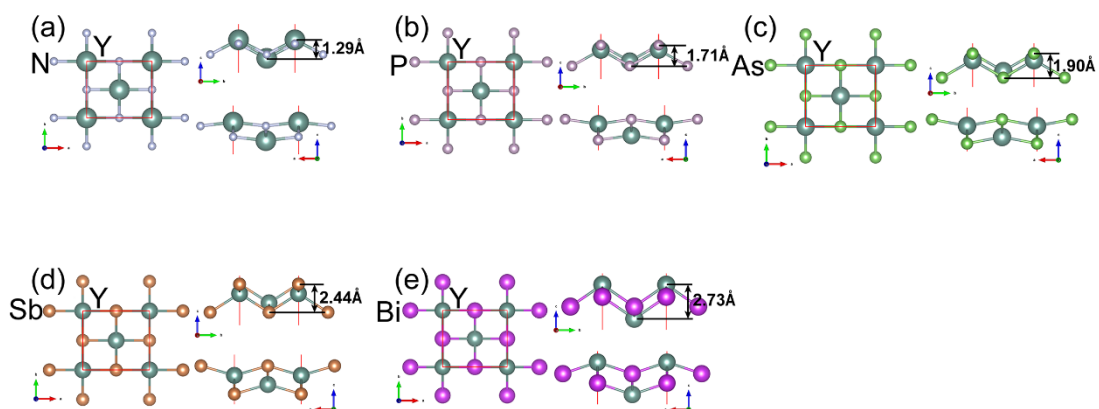**Figure S1.** Optimized structures of ML Sc*B* (*B*=N, P, As, Sb).

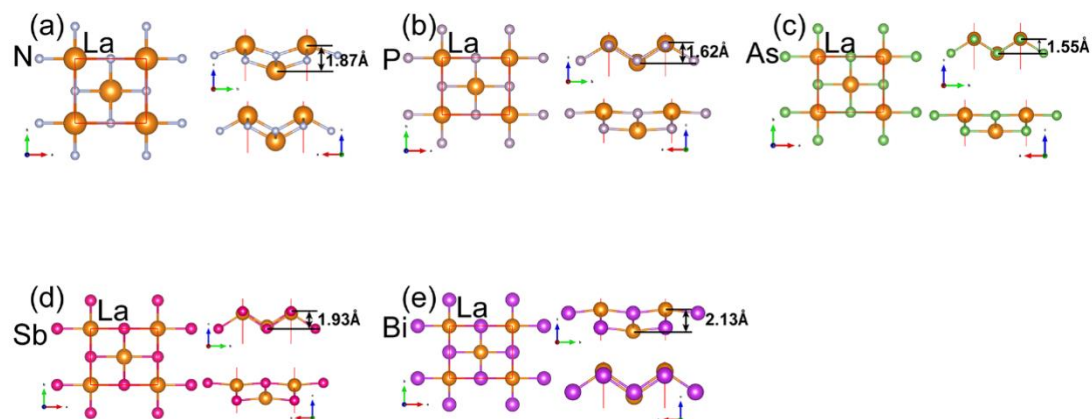**Figure S2.** Optimized structures of ML Y*B* (*B*=N, P, As, Sb, Bi).

Figure S3. Optimized structures of ML La*B* (*B*=N, P, As, Sb, Bi).
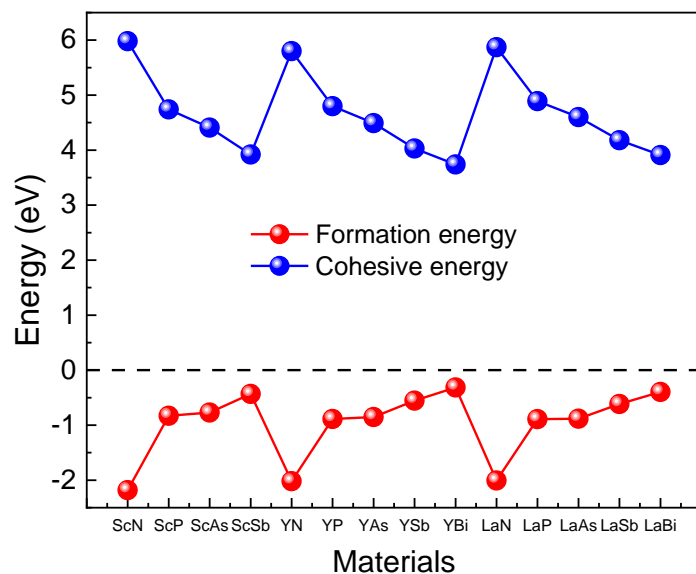
Figure S4. The calculated formation energies and cohesive energies of ML *AB* (*A* = Sc, Y, La; *B* = N, P, As, Sb, Bi).
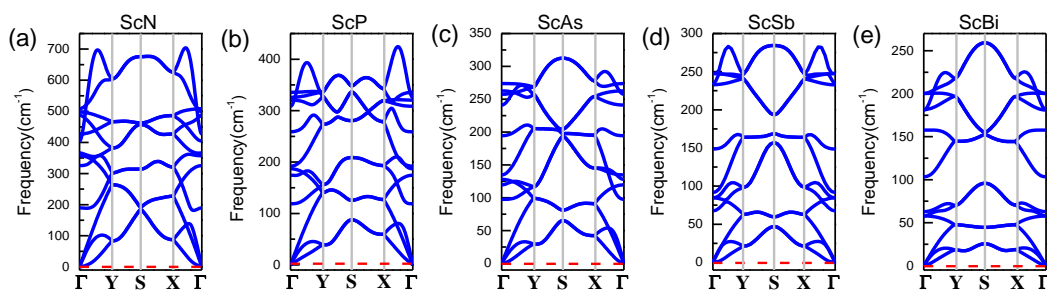
Figure S5. Calculated phonon spectra of ML Sc*B* (*B*=N, P, As, Sb and Bi).
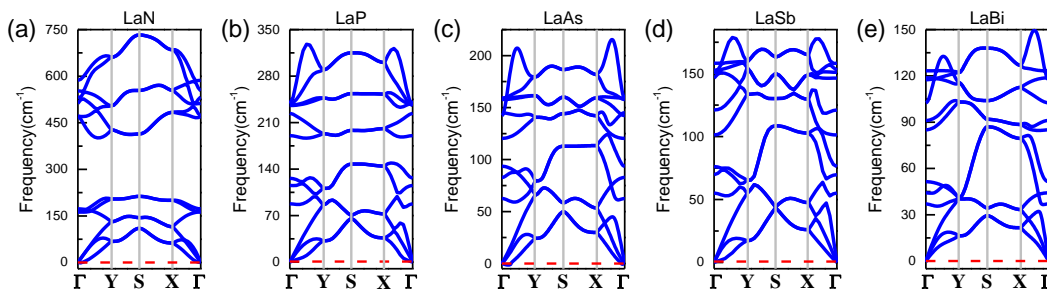
Figure S6. Calculated phonon spectra of ML La*B* (*B*=N, P, As, Sb and Bi).

Figure S7. Total energy variations as well as the top view of the snapshots from the *ab initio* molecules dynamics simulation for ML Sc*B* (*B*=N, P, As and Sb).

Figure S8. Total energy variations as well as the top view of the snapshots from the *ab initio* molecules dynamics simulation for ML Y*B* (*B*=N, P, As, Sb and Bi).
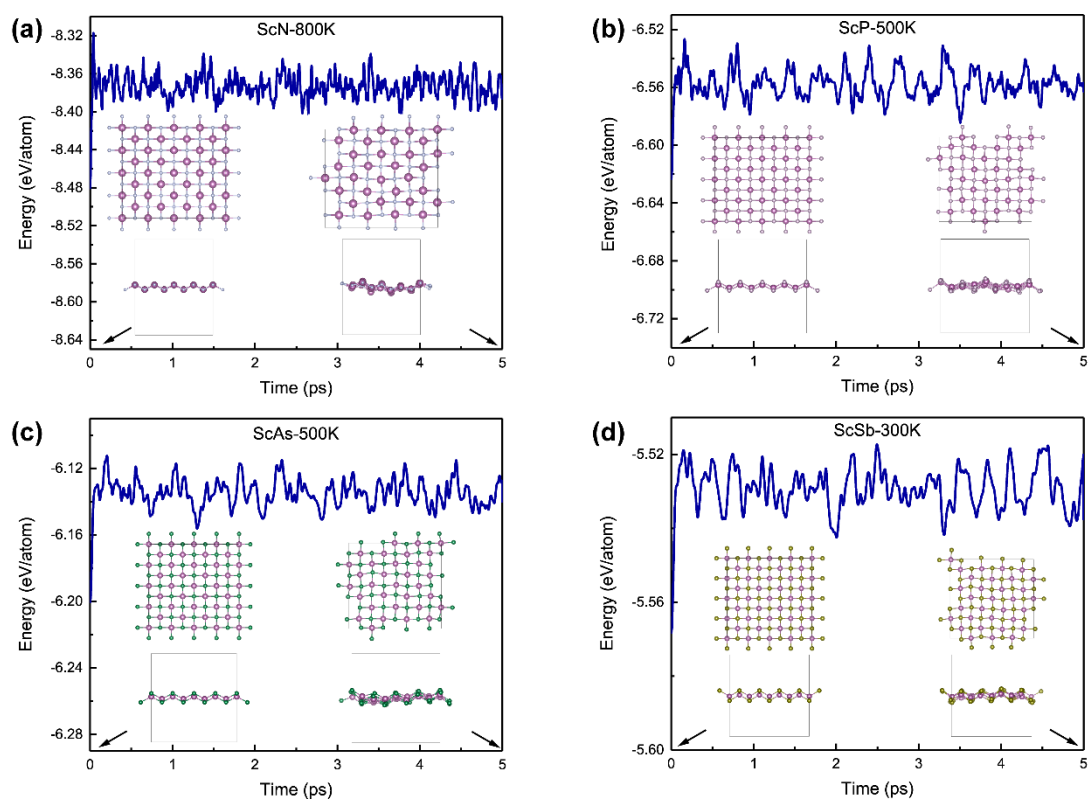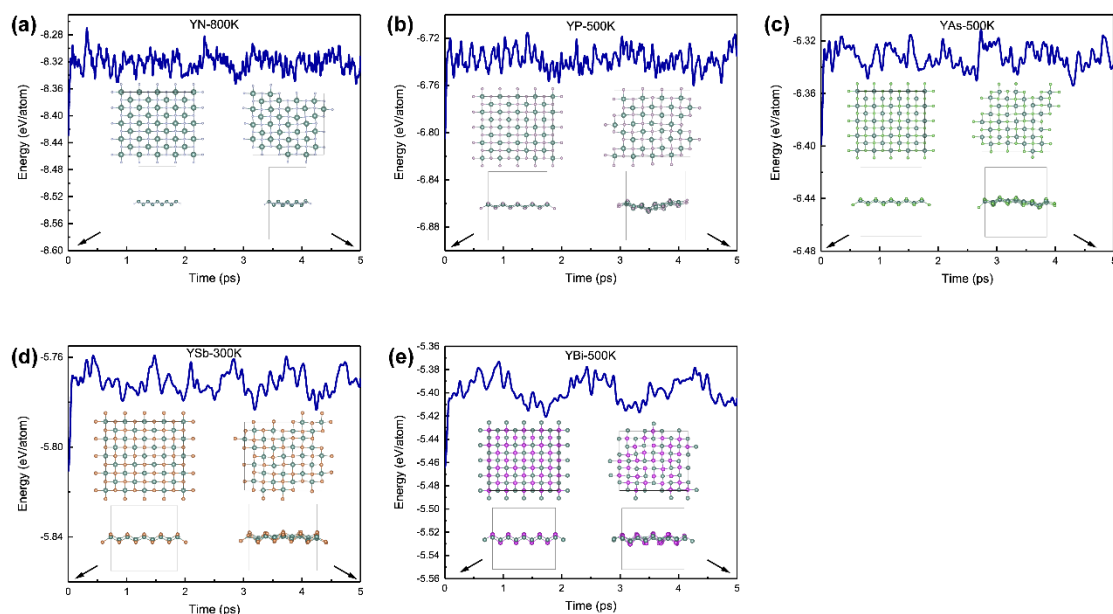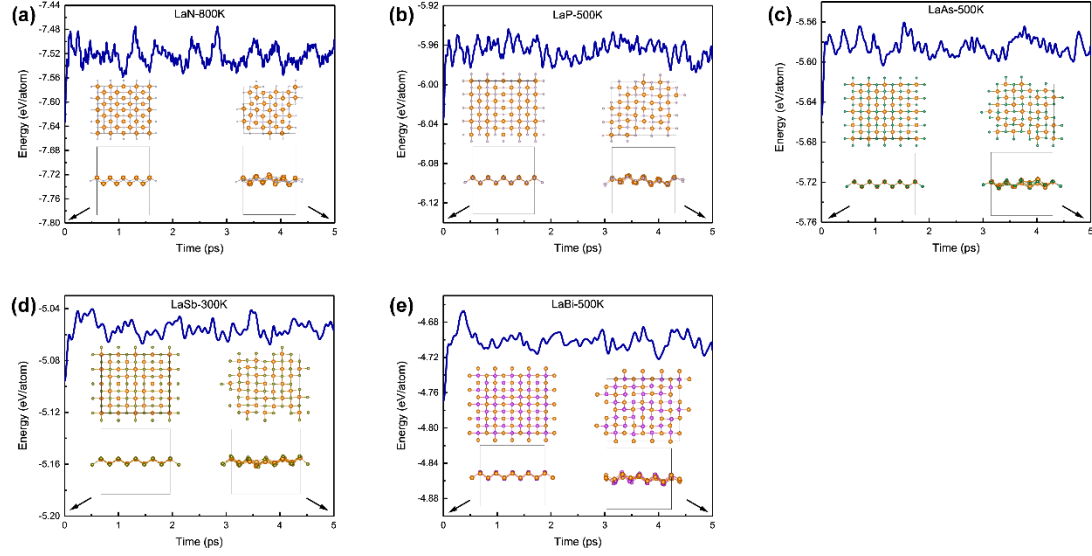
Figure S9. Total energy variations as well as the top view of the snapshots from the *ab initio* molecules dynamics simulation for ML La*B* (*B*=N, P, As, Sb and Bi).

Table S1. Calculated elastic constant of *AB* MLs. The mechanical stability is confirmed by the Born−Huang criteria, i.e. $C_{11}C_{22} - C_{12}^2 > 0$, $C_{66} > 0$.

Structure	C_{11}	C_{22}	C_{12}	C_{66} (>0)	$C_{11}C_{22} - C_{12}^2$	Mechanical stability
ScN	158.15	40.03	7.93	8.38	6268.89	Yes
ScP	72.79	10.30	12.99	23.15	581.22	Yes
ScAs	49.41	8.84	14.14	20.20	237.04	Yes
ScSb	20.96	7.29	10.23	13.29	48.12	Yes
ScBi	9.39	8.88	10.80	12.14	**-33.20**	**No**
YN	80.61	37.56	9.21	47.28	2943.23	Yes
YP	97.07	10.78	7.55	21.19	989.41	Yes
YAs	77.07	8.86	7.93	18.64	619.95	Yes
YSb	44.66	6.34	6.99	12.81	234.64	Yes
YBi	35.46	5.80	6.12	11.24	168.38	Yes
LaN	43.14	23.96	18.63	37.17	686.47	Yes
LaP	64.48	11.53	3.17	14.22	733.70	Yes
LaAs	75.50	9.53	1.43	12.40	717.35	Yes
LaSb	76.99	5.69	1.40	8.42	436.03	Yes
LaBi	69.54	221.45	66.57	7.38	10968.82	Yes

.
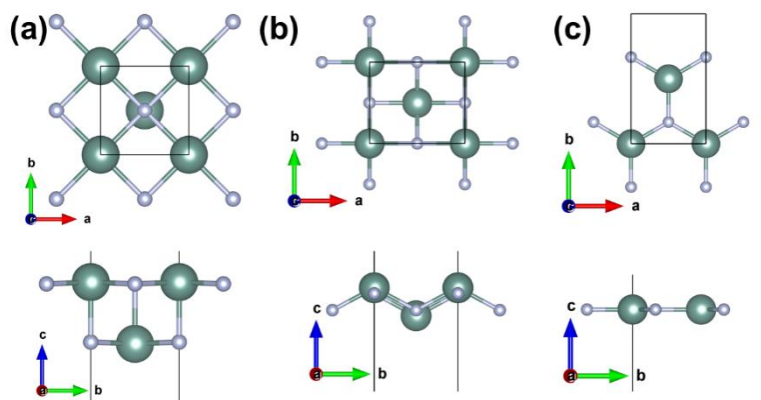
Figure S10. Optimized crystal structures of (a) YN (100), (b) YN (110) in this work and (c) YN (111).

Table S2. The cohesive energies of ML YB (B = N, P, As, Sb and Bi) with three different 2D structures taken from the *fcc* bulk, over the (100), (110) and (111) planes. The corresponding optimized structures are shown in **Figure R10**.

Cohesive energy (eV)			
Structure	100	110	111
YN	6.146	5.787	5.544
YP	5.200	4.796	4.331
YAs	4.866	4.484	4.009
YSb	4.374	4.029	3.516
YBi	4.057	3.737	3.221

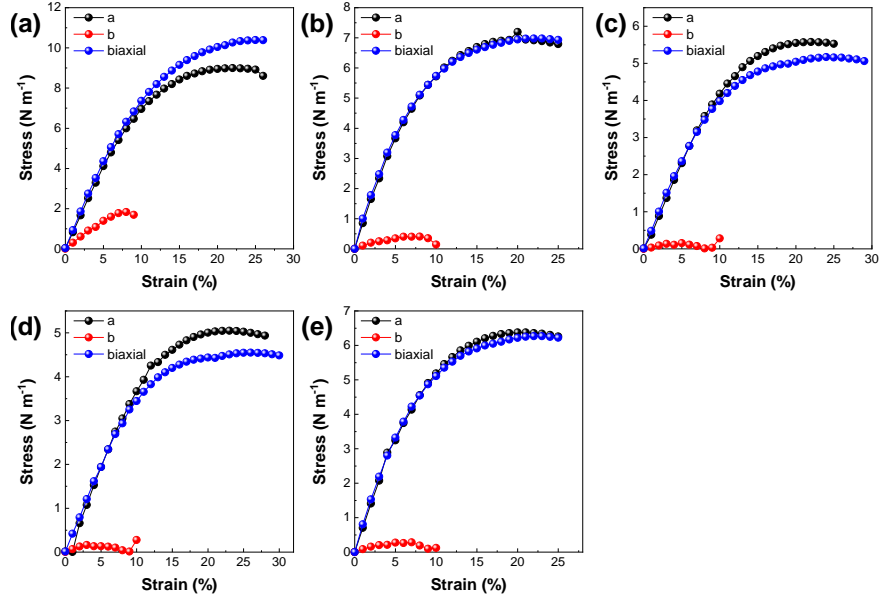**Figure S11.** The strain-stress relations of ML Y*B* (*B* = N, P, As, Sb and Bi) under uniaxial *a*, *b* and biaxial tension. (a)YN; (b) YP; (c) YAs; (d) YSb and (e) YBi.

Table S3. Summary of the ideal tensile strengths and critical strains of ML Y*B* under three strain paths.

Structures	Direction	Ideal tensile strength (N m^{-1})	Critical strain (ε)
YN	a	8.99	0.22
	b	1.83	0.08
	biaxial	10.39	0.25
YP	a	7.19	0.20
	b	0.41	0.08
	biaxial	6.98	0.22
YAs	a	6.38	0.20
	b	0.28	0.07
	biaxial	6.27	0.23
YSb	a	5.58	0.22
	b	0.15	0.05
	biaxial	5.17	0.24
YBi	a	5.05	0.23
	b	0.16	0.03
	biaxial	4.55	0.26

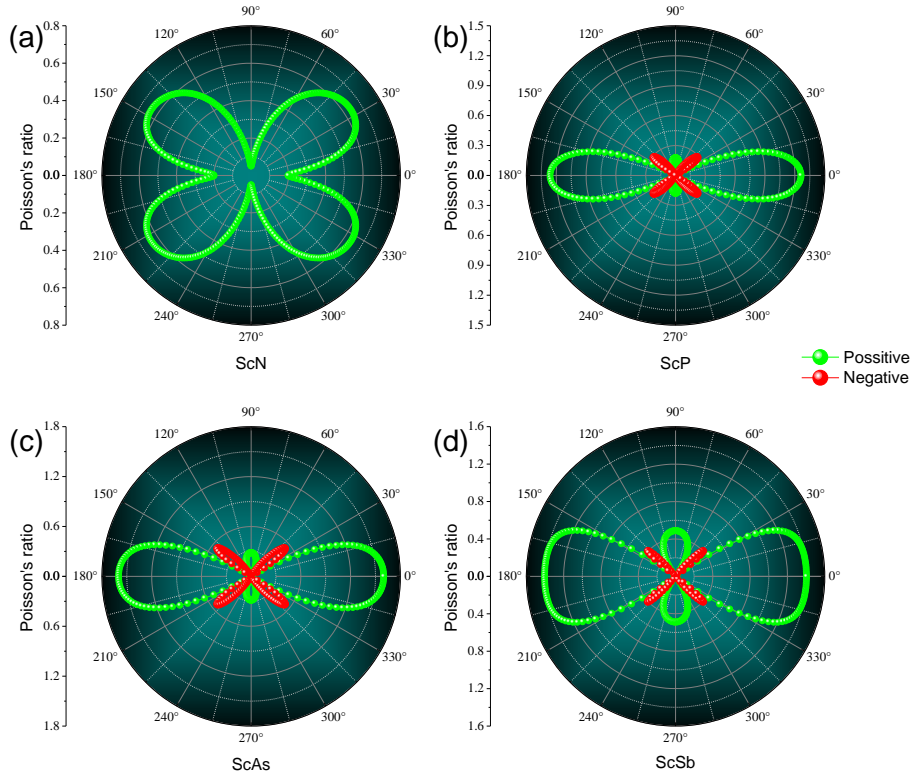**Figure S12.** (a) Poisson's ratio of ML Sc*B* (*B*=N, P, As, Sb) as a function of the angle θ, where θ = 0° corresponds to the a-axis. Negative Poisson's ratio is specially marked with red balls.

Figure S13. (a) Poisson's ratio of ML La*B* (*B*=N, P, As, Sb, BI) as a function of the angle θ, where θ = 0° corresponds to the *a*-axis. Negative Poisson's ratio is specially marked with red balls.

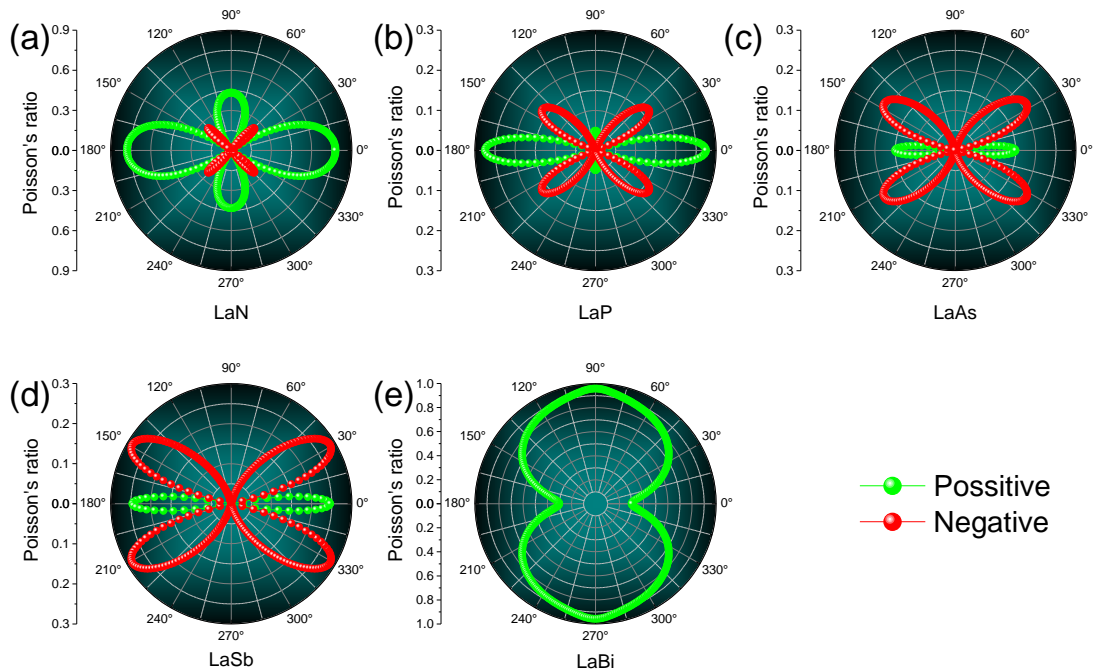**Figure S14.** The *z*-axis mechanical responses of ML *AB* under uniaxial strains. (a) ScN under uniaxial strain along the *a*-direction; (b) ScN under uniaxial strain along the *b*-direction; (c) ScP under uniaxial strain along the *a*-direction; (d) ScP under uniaxial strain along the *b*-direction; (e) ScAs under uniaxial strain along the *a*-direction; (f) ScAs under uniaxial strain along the *b*-direction; (g) ScSb under uniaxial strain along the *a*-direction; (h) ScSb under uniaxial strain along the *b*-direction.
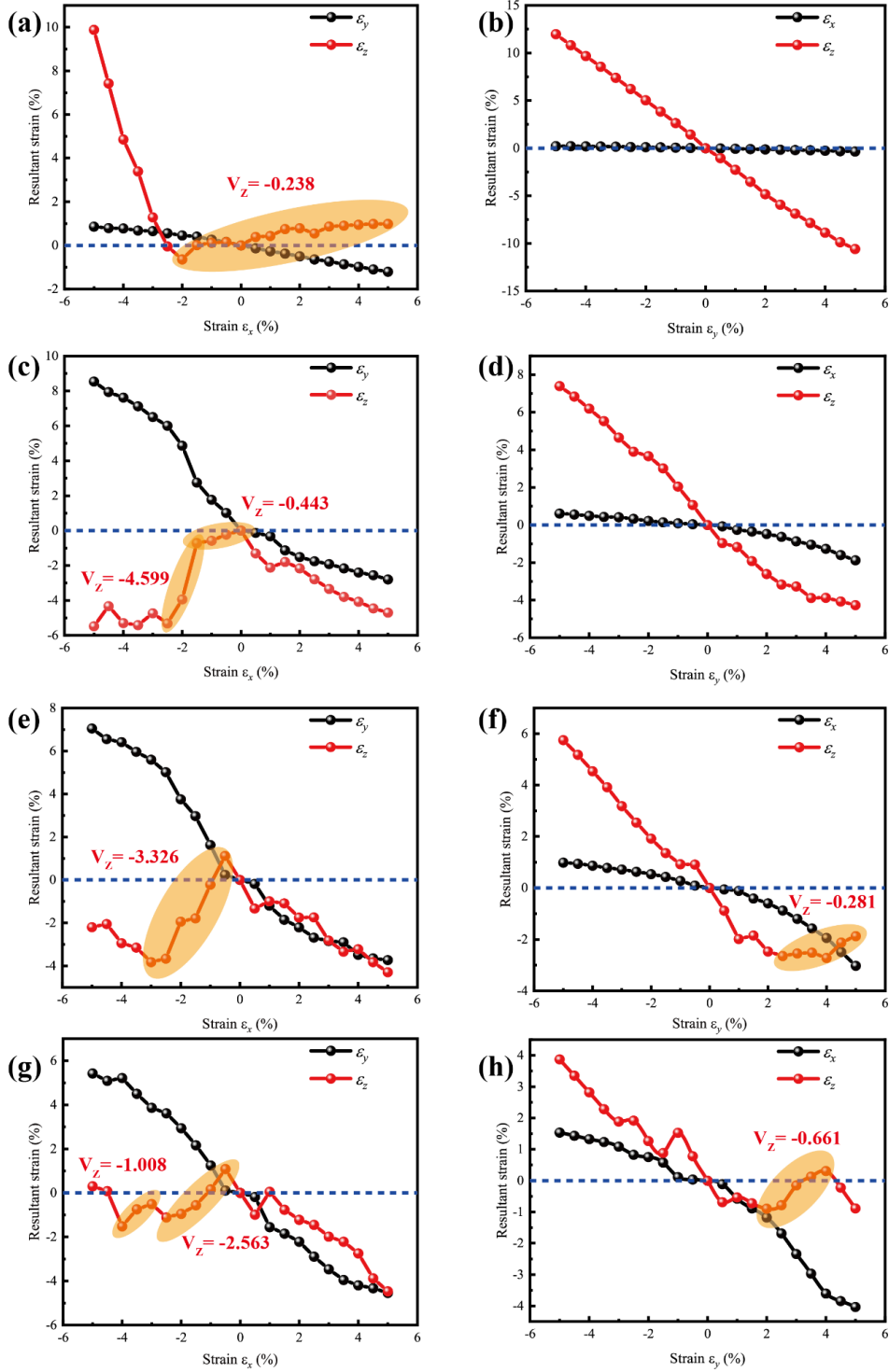
Figure S15. The *z*-axis mechanical responses of ML *AB* under uniaxial strains. (a) YN under uniaxial strain along the *a*-direction; (b) YN under uniaxial strain along the *b*-direction; (c) YP under uniaxial strain along the *a*-direction; (d) YP under uniaxial strain along the *b*-direction; (e) YAs under uniaxial strain along the *a*-direction; (f) YAs under

uniaxial strain along the *b*-direction; (g) YSb under uniaxial strain along the *a*-direction; (h) YSb under uniaxial strain along the *b*-direction. (i) YBi under uniaxial strain along the *a*-direction; (j) YBi under uniaxial strain along the *b*-direction.

Figure S16. The *z*-axis mechanical responses of ML *AB* under uniaxial strains. (a) LaN under uniaxial strain along the *a*-direction; (b) LaN under uniaxial strain along the *b*-

direction; (c) LaP under uniaxial strain along the *a*-direction; (d) LaP under uniaxial strain along the *b*-direction; (e) LaAs under uniaxial strain along the *a*-direction; (f) LaAs under uniaxial strain along the *b*-direction; (g) LaSb under uniaxial strain along the *a*-direction; (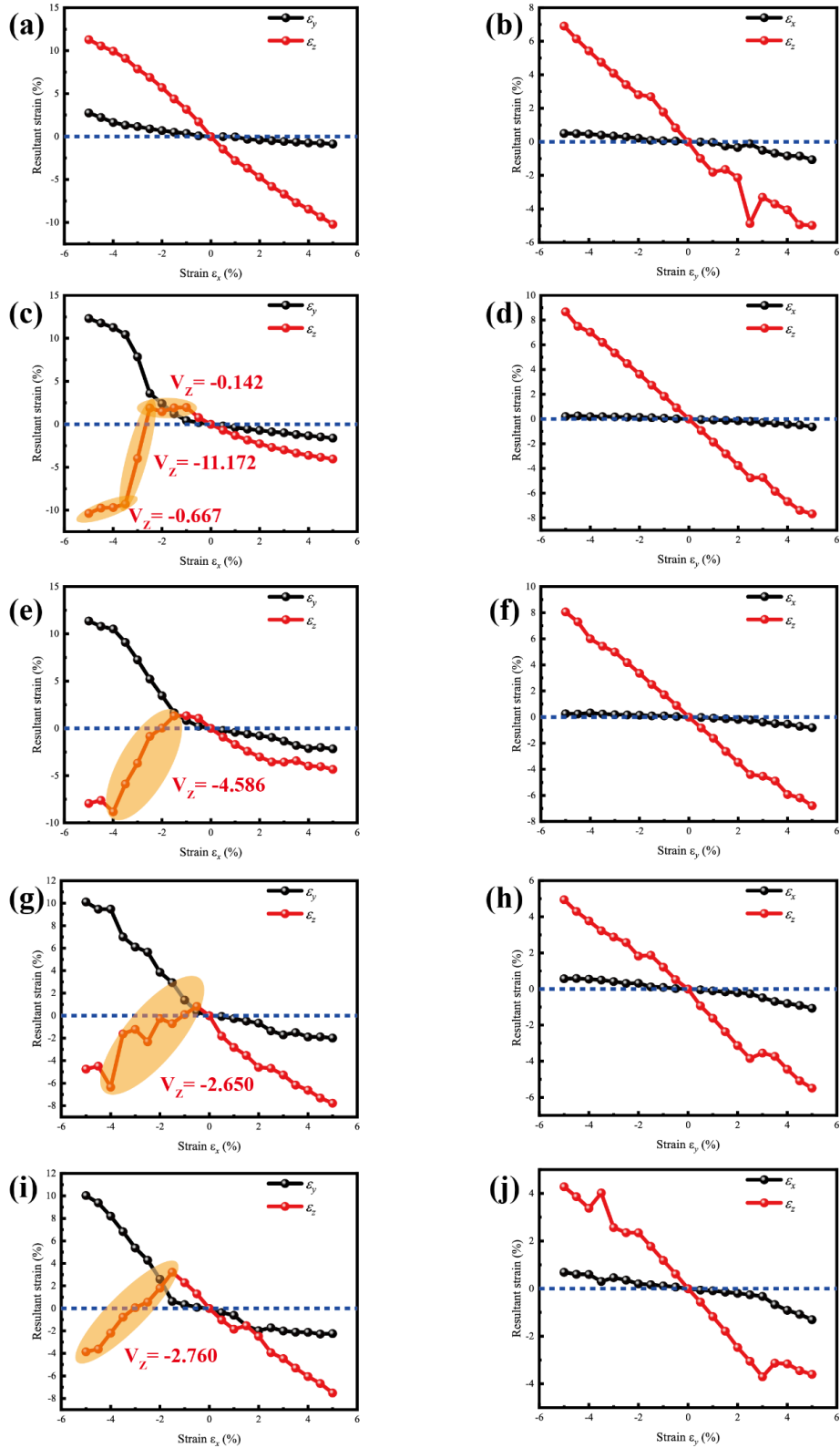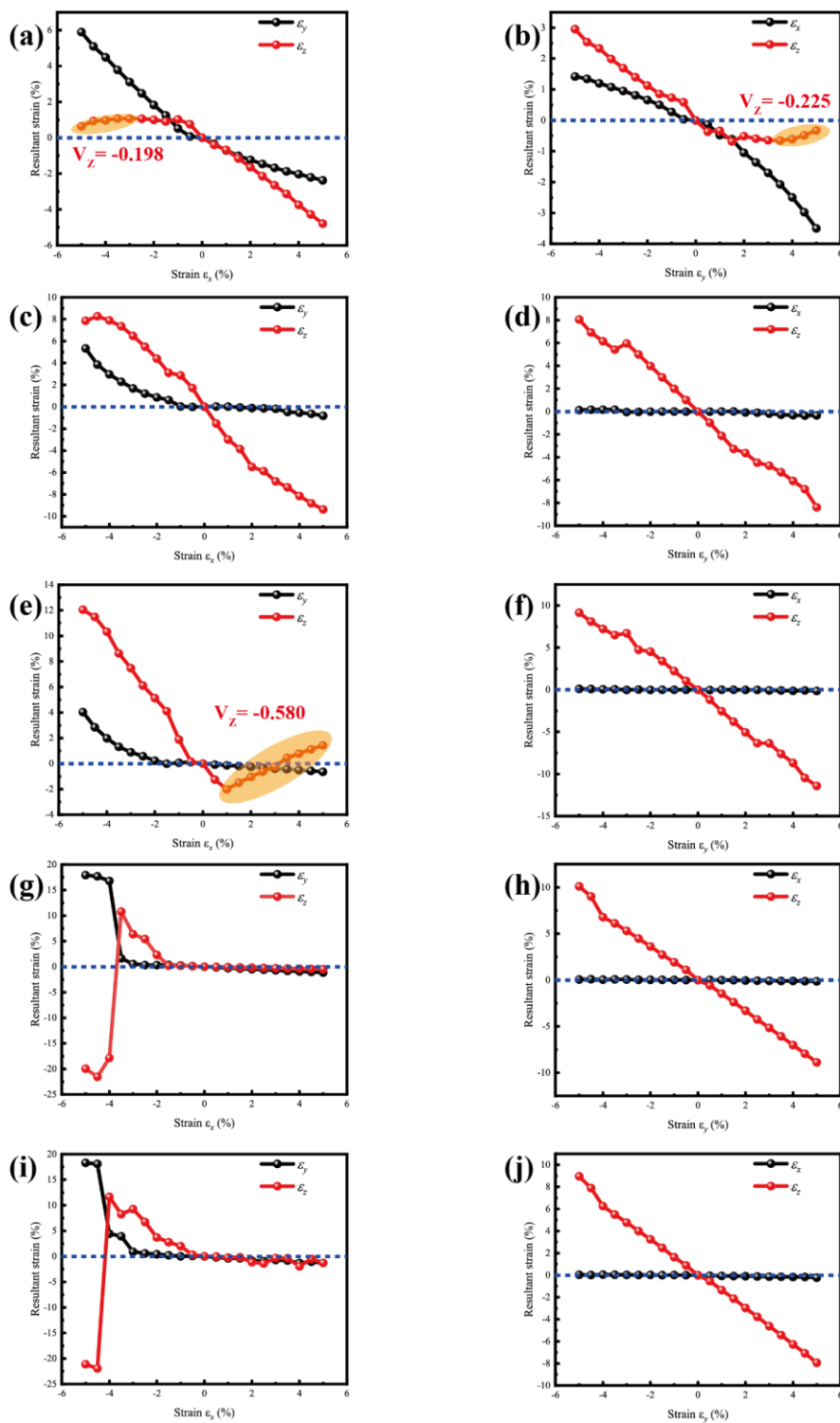h) LaSb under uniaxial strain along the *b*-direction. (i) LaBi under uniaxial strain along the *a*-direction; (j) LaBi under uniaxial strain along the *b*-direction. For (g) and (i), there is a positive slope at the red line on the left (from -4.5% to -3.5%), which was not subject to fitting because the material has undergone a phase transition.

Out-of-plane NPR calculations:

The strain is defined as $\varepsilon = (l - l_0)/l_0$, where ε involves ε_x, ε_y, and ε_z, which correspond to the relative strains along the *a*-, *b*-, and *c*-directions, respectively; $l = a, b$ represent the lattice parameters along the *a*- and *b*-directions under strain, while $l = h$ represents the buckling height (or thickness) of ML *AB* under strain; $l_0 = a_0, b_0, h_0$ are the corresponding lattice constants and buckling heights of ML *AB* without strain, respectively. In the calculations, a step size of 0.05% was used in order to get more accurate results. Upon fitting $y = -v_1x + v_2x^2 + v_3x^3$, where *y* and *x* indicate applied strain and resultant strain, v_1 is the obtained Poisson's ratio.[1] In the meantime, piecewise fitting was used to get a more reasonable result. In sum, 10 of the 14 systems exhibit out-of-plane NPR, except LaP, LaSb, LaBi and YN.

Table S4. The energy barrier E_b (meV per atom), reversible strain (%) of selected 2D ferroelastic materials. Spontaneous lattice strain η_y, initial lattice parameter a (Å), b (Å) and intermediate lattice parameters a'/b' (Å) are also listed.

| Material	a	b	$a'=b'$	η_y	E_b	Strain
ScN	4.313	3.761	4.182	[0.032, 0; 0, -0.096]	43.39	14.67%
ScP	4.997	4.539	4.837	[0.034, 0; 0, -0.060]	2.53	10.80%
ScAs	5.077	4.687	4.930	[0.030, 0; 0, -0.048]	1.38	8.32%
ScSb	5.262	4.967	5.126	[0.027, 0; 0, -0.031]	0.28	5.94%
YN	4.618	3.982	4.349	[0.064, 0; 0, -0.081]	32.47	15.97%
YP	5.442	4.750	5.248	[0.038, 0; 0, -0.090]	48.58	14.59%
YAs	5.557	4.874	5.352	[0.039, 0; 0, -0.085]	8.62	14.01%
YSb	5.813	5.126	5.580	[0.043, 0; 0, -0.078]	3.95	13.40%
YBi	5.865	5.145	5.607	[0.047, 0; 0, -0.079]	5.15	14.01%
LaN	4.616	4.161	4.404	[0.049, 0; 0, -0.054]	3.15	10.94%
LaP	5.796	4.858	5.508	[0.054, 0; 0, -0.111]	32.85	19.31%
LaAs	5.978	4.993	5.726	[0.045, 0; 0, -0.120]	41.35	19.74%
LaSb	6.350	5.316	6.135	[0.036, 0; 0, -0.125]	24.76	19.46%
LaBi	6.449	5.332	6.223	[0.037, 0; 0, -0.133]	21.08	20.30%
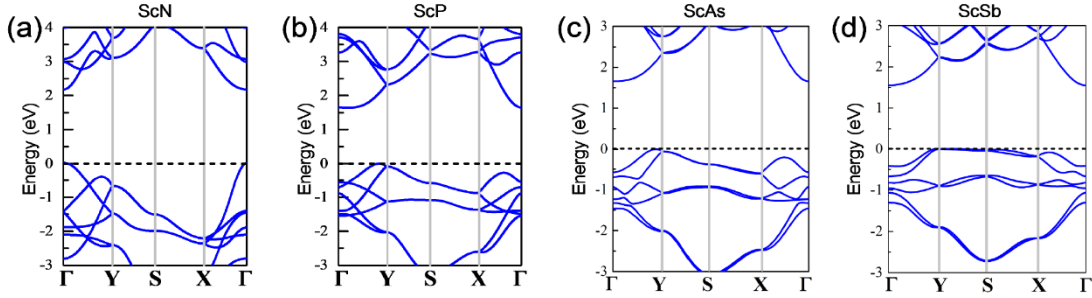
Figure S17. Electronic band structures of ScB (B=N, P, As and Sb) obtained from HSE06 hybrid functional calculations. For ScAs and ScSb, spin-orbit coupling has been considered in the hybrid functional calculations.
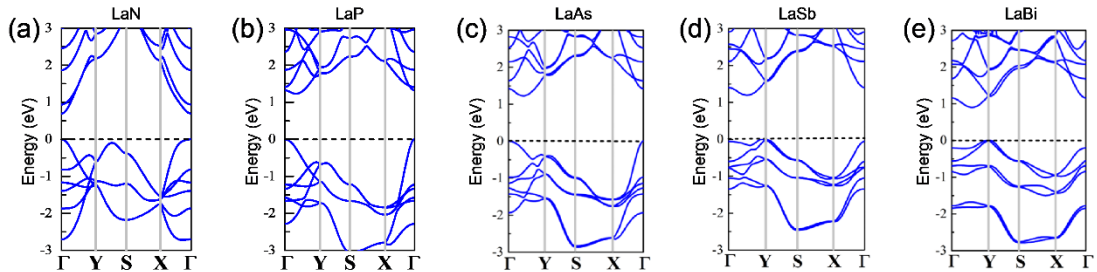

Figure S18. Electronic band structures of LaB (B=N, P, As, Sb and Bi) obtained from HSE06 hybrid functional calculations. For LaAs, LaSb and LaBi, spin-orbit coupling has been considered in the hybrid functional calculations.

Table S5. Calculated band gaps at the HSE06, HSE06+SOC and GGA+U levels (eV). For the GGA+U calculations, U=3 eV for Sc-3d,[2] U=4 eV for Y-4d and U=5.4 eV for La-5d[3] were used for on-site Hubbard corrections.

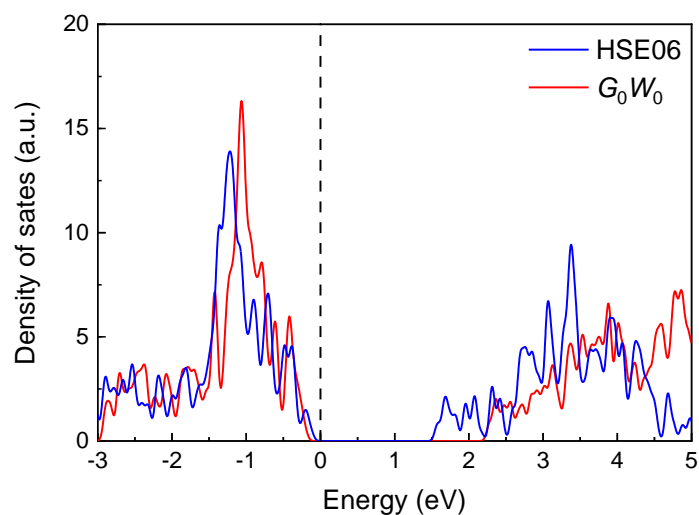|	GGA-PBE	HSE06	HSE06+SOC	GGA+U
ScN	1.30	2.15	--	1.34
ScP	0.91	1.64	--	1.12
ScAs	0.93	1.66	1.65(7)	1.12
ScSb	0.84	1.57	1.55	1.01
YN	0.004	0.75	--	0.004
YP	1.01	1.67	--	1.23
YAs	1.02	1.66	1.65	1.21
YSb	0.94	1.57	1.54	1.09
YBi	0.98	1.58	1.36	1.28
LaN	0.29	0.69	--	
LaP	0.82	1.23	--	1.06
LaAs	0.82	1.23	1.22	1.18
LaSb	0.80	1.23	1.18	1.27
LaBi	0.76	1.14	1.00	1.25

Figure S19. Density of states of ML YP at the HSE06 and G_0W_0 levels.

Table S6. Calculated band gaps of bulk and ML *AB* using HSE06 or HSE06+SOC.

Bulk/ML materials	Band gap (eV) (bulk)	Band gap (eV) (ML)
ScN	0.92	2.15
ScP	0	1.64
ScAs	0	1.65(7)
ScSb	0	1.55
YN	1.12	0.75
YP	0	1.67
YAs	0	1.65
YSb	0	1.54
YBi	0	1.36
LaN	0.84	0.69
LaP	0.13	1.23
LaAs	0	1.22
LaSb	0	1.18
LaBi	0	1.00
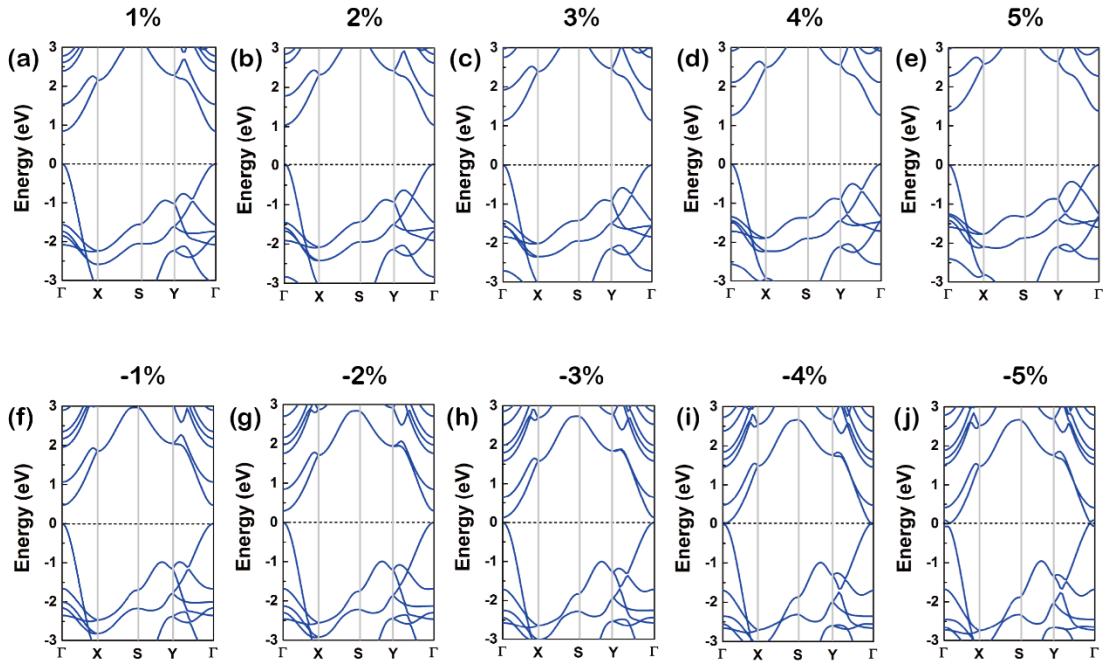
Figure S20. Electronic band structures of YN obtained from HSE06 hybrid functional calculations under biaxial strains from -5% to 5%.
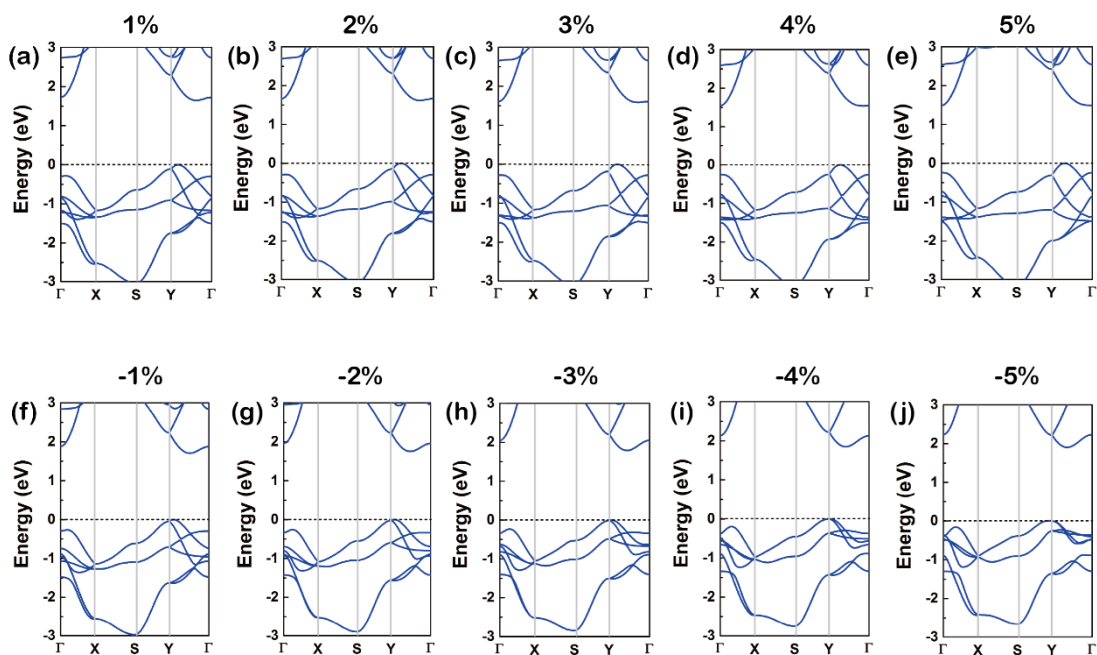
Figure S21. Electronic band structures of YP obtained from HSE06 hybrid functional calculations under biaxial strains from -5% to 5%.
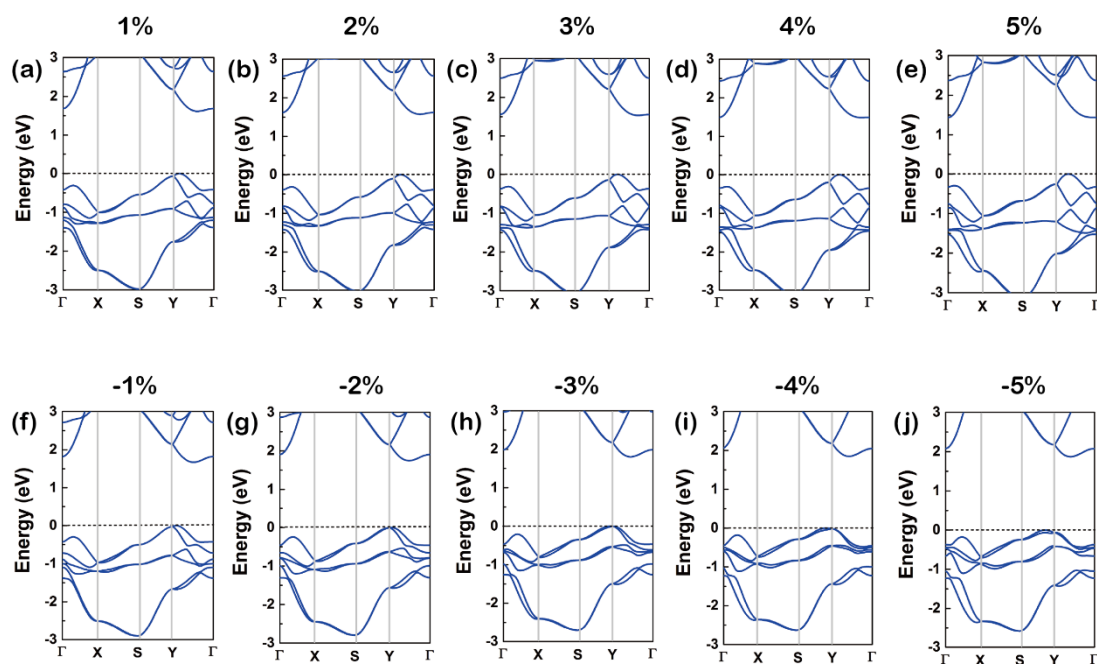

Figure S22. Electronic band structures of YAs obtained from HSE06 hybrid functional calculations under biaxial strains from -5% to 5%. In the calculations, the spin-orbit coupling effect has also been considered.

Figure S23. Electronic band structures of YSb obtained from HSE06 hybrid functional calculations under biaxial strains from -5% to 5%. In the calculations, the spin-orbit coupling effect has also been considered.
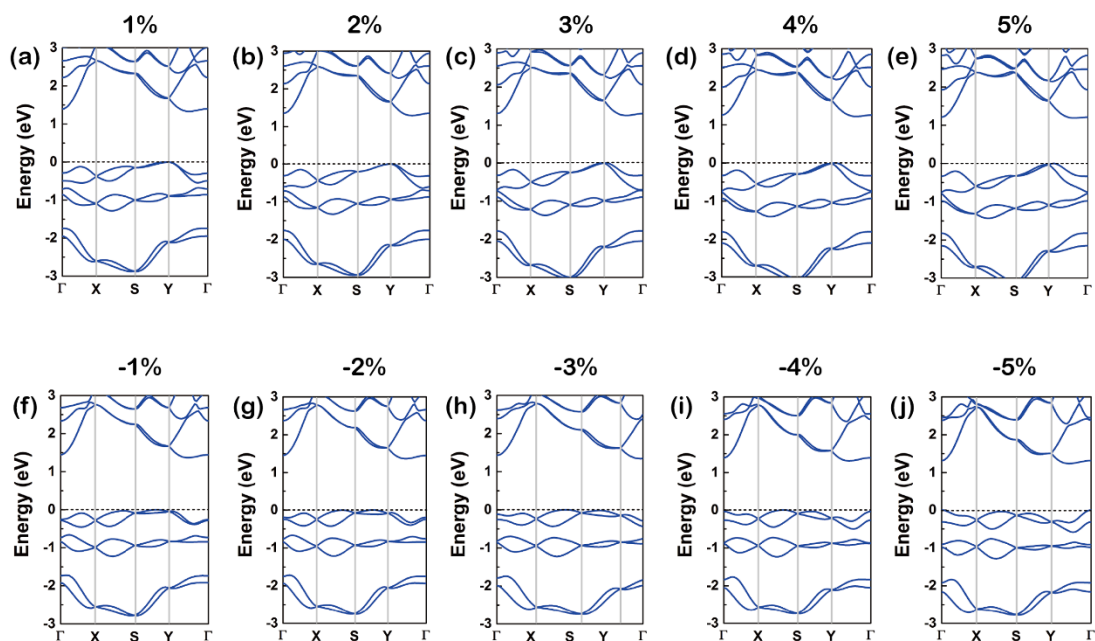
Figure S24. Electronic band structures of YBi obtained from HSE06 hybrid functional calculations under biaxial strains from -5% to 5%. In the calculations, the spin-orbit coupling effect has also been considered.
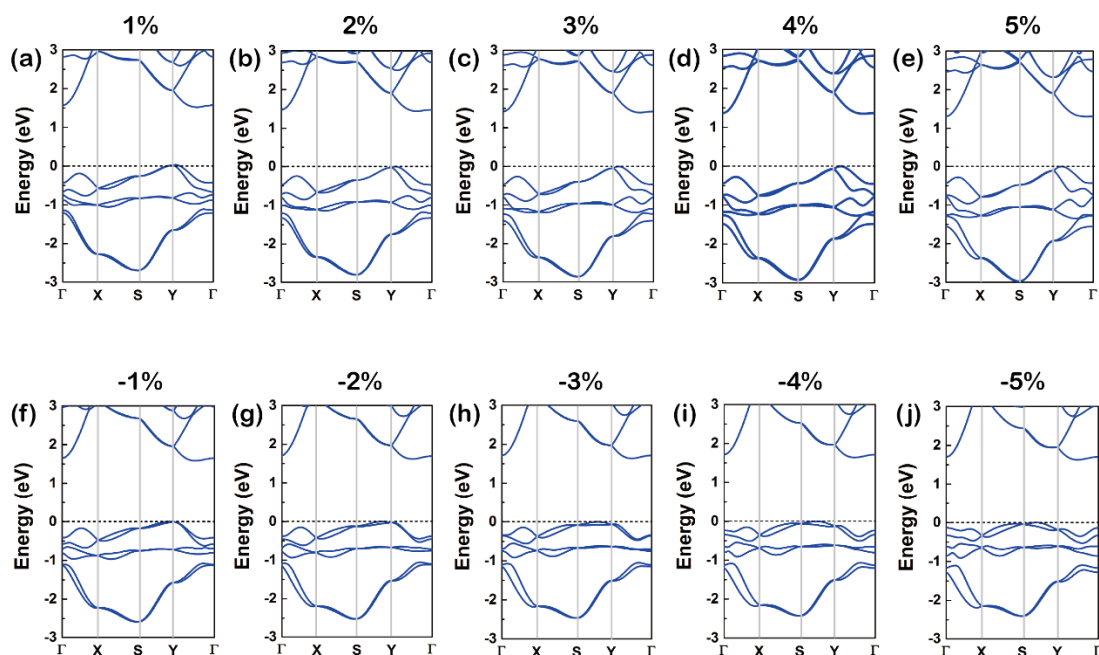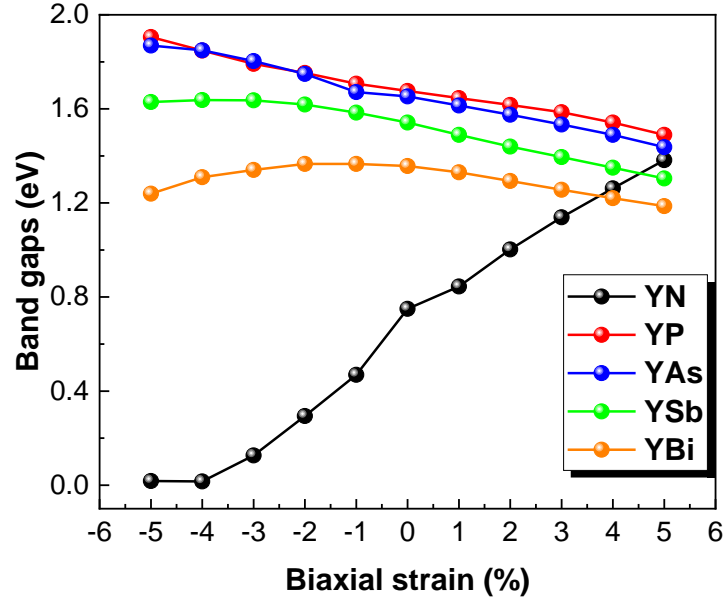
Figure S25. The corresponding electronic band gaps of Y*B* (*B* = N, P, As, Sb, Bi) obtained from HSE06 hybrid functional calculations under biaxial strains from -5% to 5%.

Figure S26. Projected density of states of ML Sc*B*. (a) ScN; (b) ScP; (c) ScAs; (d) ScSb.

Figure S27. Projected density of states of ML Y*B*. (a) YN; (b) YP; (c) YAs; (d) YSb; (e) YBi.

Figure S28. Projected density of states of ML La*B*. (a) LaN; (b) LaP; (c) LaAs; (d) LaSb; (e) LaBi.

Figure S29. The calculated cleavage energies of ML Y*B* (*B* = N, P, As, Sb and Bi).

The corresponding structure files in the VASP-POSCAR format, of these 14 materials:

ScN
1.0

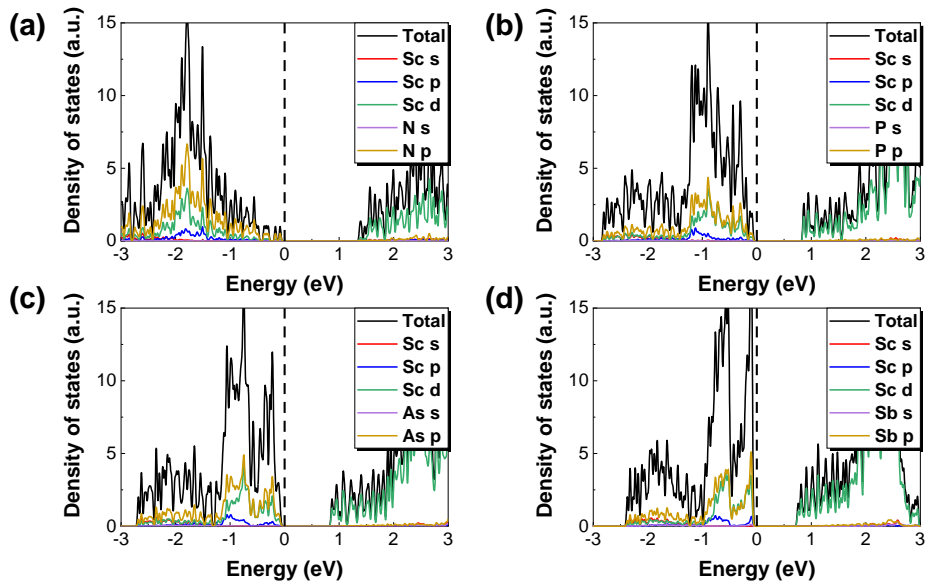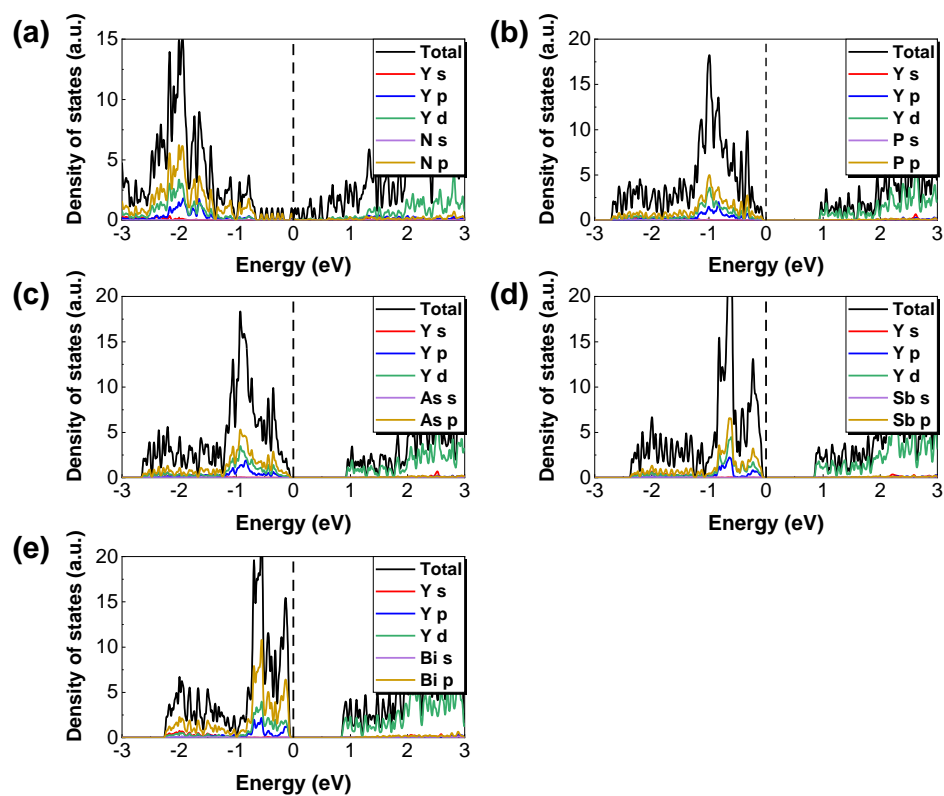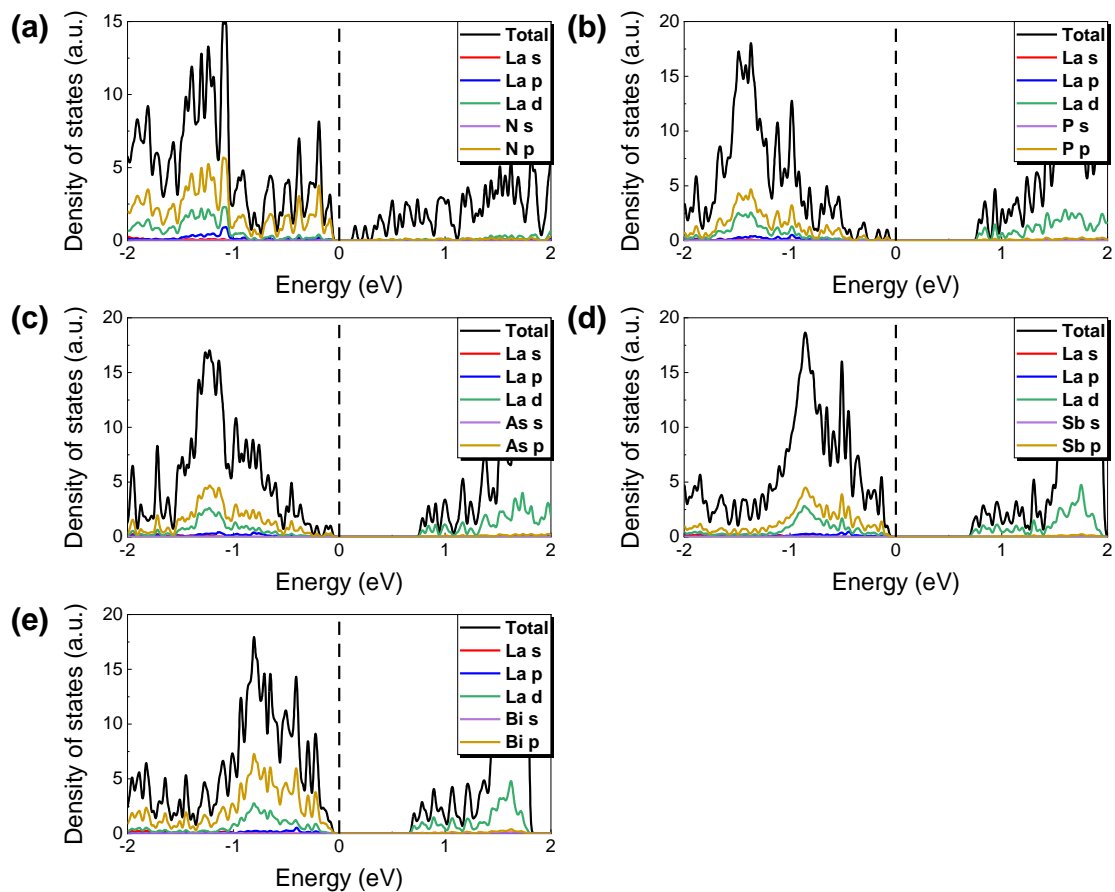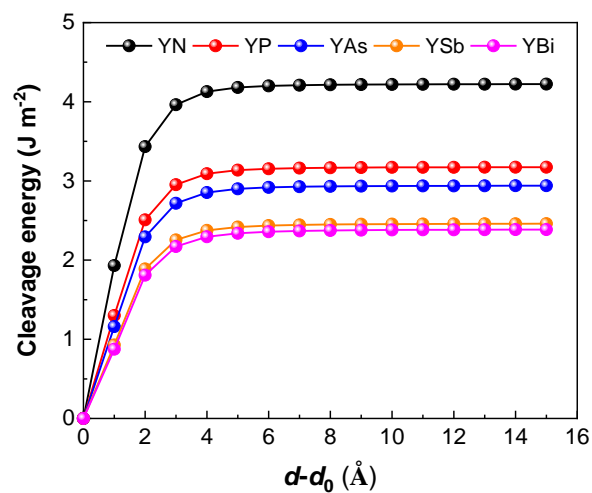|		
4.3127999306	0.0000000000	0.0000000000
0.0000000000	3.7611000538	0.0000000000
0.0000000000	0.0000000000	18.4181003571

Sc   N
2   2
Direct

0.000000000	0.000000000	0.523949998
0.500000000	0.500000000	0.476050002
0.500000000	0.000000000	0.525960015
0.000000000	0.500000000	0.474039985

ScP
1.0

4.9967999458	0.0000000000	0.0000000000
0.0000000000	4.5391001701	0.0000000000
0.0000000000	0.0000000000	19.2161998749

Sc   P
2   2
Direct

0.000000000	0.000000000	0.515600026
0.500000000	0.500000000	0.484399974
0.500000000	0.000000000	0.545689984
0.000000000	0.500000000	0.454310016

ScAs
1.0

5.0766000748	0.0000000000	0.0000000000
0.0000000000	4.6865000725	0.0000000000
0.0000000000	0.0000000000	19.4174995422

Sc   As
2   2
Direct

0.000000000	0.000000000	0.512530006
0.500000000	0.500000000	0.487469994
0.500000000	0.000000000	0.550729974
0.000000000	0.500000000	0.449270026

YN
1.0
4.6180000305	0.0000000000	0.0000000000
0.0000000000	3.9820001125	0.0000000000
0.0000000000	0.0000000000	30.8400001526

Y   N
2   2
Direct
0.000000000	0.000000000	0.521120012
0.500000000	0.500000000	0.478879988
0.500000000	0.000000000	0.512380004
0.000000000	0.500000000	0.487619996

YP
1.0
5.4419598578999997	0.0000000000000000	0.0000000000000000
0.0000000000000000	4.7492198944000004	0.0000000000000000
0.0000000000000000	0.0000000000000000	22.0035991668999991

Y   P
2   2
Direct
0.0000000000000000	0.0000000000000000	0.5212649699999972
0.5000000000000000	0.5000000000000000	0.4787350000000004
0.5000000000000000	0.0000000000000000	0.5388529900000023
0.0000000000000000	0.5000000000000000	0.4611470099999977

YAs
1.0
5.5570402144999997	0.0000000000000000	0.0000000000000000
0.0000000000000000	4.8740000725000003	0.0000000000000000
0.0000000000000000	0.0000000000000000	22.0035991668999991

Y   As
2   2
Direct
0.0000000000000000	0.0000000000000000	0.5200570229999997
0.5000000000000000	0.5000000000000000	0.4799430070000028
0.5000000000000000	0.0000000000000000	0.5434430239999983
0.0000000000000000	0.5000000000000000	0.4565570059999970

YSb
1.0
5.8130663275071361   0.0000000000000000   0.0000000000000000
0.0000000000000000   5.1260802381166917   0.0000000000000000
0.0000000000000000   0.0000000000000000   20.0049495696999990
Y   Sb
2   2
Direct
0.0000000000000000   0.0000000000000000   0.5198718064235095
0.5000000000000000   0.5000000000000000   0.4801282235764859
0.5000000000000000   0.0000000000000000   0.5610252687503774
0.0000000000000000   0.5000000000000000   0.4389747612496251

YBi
1.0
5.8653149118919137   0.0000000000000000   0.0000000000000000
0.0000000000000000   5.1446326843952006   0.0000000000000000
0.0000000000000000   0.0000000000000000   20.3881607056000007
Y   Bi
2   2
Direct
0.5000000000000000   0.0000000000000000   0.5193660274754777
0.0000000000000000   0.5000000000000000   0.4806339613538952
0.0000000000000000   0.0000000000000000   0.5669285571855553
0.5000000000000000   0.5000000000000000   0.4330714839850742

LaN
1.0
4.6160001755   0.0000000000   0.0000000000
0.0000000000   4.1607999802   0.0000000000
0.0000000000   0.0000000000   21.5841999054
La   N
2   2
Direct
0.000000000   0.000000000   0.543349982
0.500000000   0.500000000   0.456650018
0.500000000   0.000000000   0.508639987
0.000000000   0.500000000   0.491360013

LaP
1.0
5.7955999374	0.0000000000	0.0000000000
0.0000000000	4.8576002121	0.0000000000
0.0000000000	0.0000000000	20.2600994110

La   P
2   2
Direct
0.000000000	0.000000000	0.540050030
0.500000000	0.500000000	0.459949970
0.500000000	0.000000000	0.531899967
0.000000000	0.500000000	0.468100033

LaAs
1.0
5.9779000282	0.0000000000	0.0000000000
0.0000000000	4.9925999641	0.0000000000
0.0000000000	0.0000000000	20.0849990845

La   As
2   2
Direct
0.000000000	0.000000000	0.538600047
0.500000000	0.500000000	0.461399953
0.500000000	0.000000000	0.537230004
0.000000000	0.500000000	0.462769996

LaSb
1.0
6.3501000404	0.0000000000	0.0000000000
0.0000000000	5.3154997826	0.0000000000
0.0000000000	0.0000000000	19.7266998291

La   Sb
2   2
Direct
0.000000000	0.000000000	0.536119991
0.500000000	0.500000000	0.463880009
0.500000000	0.000000000	0.548870038
0.000000000	0.500000000	0.451129962

LaBi
1.0
```
6.4496998787        0.0000000000        0.0000000000
0.0000000000        5.3614997864        0.0000000000
0.0000000000        0.0000000000       19.7647991180
```
La   Bi
2   2
Direct
```
0.500000000        0.000000000        0.535769978
0.000000000        0.500000000        0.464230022
0.000000000        0.000000000        0.553909998
0.500000000        0.500000000        0.446090002
```

References

[1]   J.-H. Yuan, K.-H. Xue, J.-F. Wang and X.-S. Miao, *J. Phys. Chem. Lett.*, 2019, **10**, 4455–4462.

[2]   F. Kang, H. Zhang, L. Wondraczek, X. Yang, Y. Zhang, D. Y. Lei and M. Peng, *Chem. Mater.*, 2016, **28**, 2692–2703.

[3]   H. Jiang, R. I. Gomez-Abal, P. Rinke and M. Scheffler, *Phys. Rev. Lett.*, 2009, **102**, 126403.